

Coherence and Decoherence in Biological Systems: Principles of Noise Assisted Transport and the Origin of Long-lived Coherences

A. W. Chin, S. F. Huelga and M. B. Plenio

Institute of Theoretical Physics, Universität Ulm, Albert-Einstein-Allee 11, 89069 Ulm, Germany

The quantum dynamics of transport networks in the presence of noisy environments have recently received renewed attention with the discovery of long-lived coherences in different photosynthetic complexes. This experimental evidence has raised two fundamental questions: Firstly, what are the mechanisms supporting long-lived coherences and secondly, how can we assess the possible functional role that the interplay of noise and quantum coherence might play in the seemingly optimal operation of biological systems under natural conditions? Here we review recent results, illuminate them at the hand of two paradigmatic systems, the Fenna-Matthew-Olson (FMO) complex and the light harvesting complex LHII, and present new progress on both questions. In particular we introduce the concept of the phonon antennae and discuss the possible microscopic origin of long-lived electronic coherences.

I. BACKGROUND & MOTIVATION

Quantum mechanics provides the natural laws that govern the dynamical evolution of atoms and molecules. Under well controlled conditions in almost perfectly isolated systems, quantum coherence and entanglement can exist and be manipulated. While there is a clear notion of sub-systems when individual units are spatially well separated, as is usually the case in systems suitable for quantum information processing, this is not necessarily so in molecular complexes, where partitioning the total systems by means of the choice of appropriate subsystems is, to some extent, arbitrary. In such situations, when the system is static, coherence and entanglement can always be made to vanish in a suitably chosen basis [1, 2]. Hence, to observe non-trivial quantum effects we need to force the system out of its preferred eigenbasis, through intervention from the outside, and thus probe quantum coherences between eigenstates, as well as the quantum coherence properties of their consequent dynamics. We can then argue that, while the *static* system can *sustain* quantum coherence, it is the dynamics generated by the external perturbation which results in relevant quantum phenomena and provides the means to probe for interesting quantum properties.

The external perturbation may either be coherent and controlled, for example through the action of laser fields, or it may be caused by an interaction with an unobserved environment. The latter will never be completely avoidable, as perfect isolation of a physical system from its environment is impossible. In fact, in bio-molecular complexes the interaction with uncontrolled environments such as vibrations of the surrounding protein matrix, for example in the form of thermal fluctuations, is an important driving force of its energetic dynamics and hence its functionality. One may therefore expect that the interplay between the internal coherent quantum dynamics of the system and the unavoidable presence of noise introduced by the environment has been optimized by Nature during evolution and may be significant for its function.

Exploring to what extent coherent quantum dynamics

play a role in composite quantum systems in contact with environments, such as bio-molecular complexes and, importantly, what role, if any, genuine quantum traits may play is thus an interesting and timely problem. Exploring these issues becomes particularly challenging in those bio-molecular systems where the strength and timescales associated with the environment-induced dynamics dynamics are often comparable to the coherent (Hamiltonian) intra-system dynamics, and cannot therefore be treated separately.

The investigation of these types of questions has gained further urgency with the recent discovery of experimental evidence that excitation energy transport dynamics in the Fenna-Matthew-Olson (FMO) complex and other photosynthetic aggregates exhibits surprisingly long-lived coherence [3–5]. The FMO complex is an example of a pigment-protein complex, a network through which electronic excitations on individual pigments can migrate via excitonic couplings. These experiments suggest the existence of significant quantum coherences between multiple pigments through the presence of oscillations in the cross-peaks of 2-D spectra which have been observed to persist on timescales up to around a picosecond [5]. This is notable given that the entire excitation energy transport in the FMO complex is concluded in less than 5ps.

Theoretical investigations of the role of pure dephasing noise in excitation-energy transfer have found that this noise mechanism has the ability to enhance both the rate and yield of excitation-energy transfer when compared to perfectly coherent evolution [6, 7]. An often quoted argument states that in the exciton basis typically used in previous studies [8], noise-assisted transport is trivially explained as the result of noise-induced transitions between exciton eigenstates, which cause an energetic down-hill relaxation towards the reaction centre. While this argument can serve to suggest that noise-assisted processes might exist in excitation-energy transfer and other forms of transport in quantum networks, it falls short, as it cannot explain why in some networks noise is exclusively detrimental while in others it can support

transport. Answering such a question requires a more detailed study that identifies basic dynamical principles of quantum networks in contact with environments.

Here we would like to provide a fresh look at the problem by elucidating the basic mechanisms which give rise to noise-assisted transport and identifying where noise and coherence respectively play a constructive role [6, 7, 9–13]. Identifying and understanding these mechanisms at a deep, intuitive level does provide additional value even if the individual processes might have been known in some previous contexts. Such classifications pave the way towards tailored experimental tests of the contributions of individual processes [15]. Furthermore, quantum coherence can only be expected to be relevant if it is sufficiently long-lived. Present experiments suggest lifetimes of coherences between excited states extending up to the picosecond range while at the same time the coherence between ground and excited states are known to last for only about 50-150 fs or so. The origin of these long-lived coherences remains to be fully clarified. A complete understanding of these fundamental dynamical principles and the origin of the long-lived coherences will allow for the optimization of network architectures in order to utilize quantum coherence and noise to enhance the performance of artificial nano-structure devices.

II. PRINCIPLES OF NOISE ASSISTED TRANSPORT

In this section we will briefly review the basic dynamical principles for noise assisted transport following and extending the ideas developed in [7, 10, 12–14], and further expand them with the new concept of the *phonon antenna* by which coherent dynamics may assist the fine-tuning of the network to the spectral density of the fluctuating environment.

A. Basic dynamical principles

We have argued that both noise *and* coherence are important for the time evolution of quantum networks in the presence of an environment. But, how does the interplay between these processes occur?

1. Bridging energy gaps & blocking paths

Pigment-protein complexes will consist of a number of sites whose energies will generally exhibit a certain degree of static disorder, i.e. their on-site energies will differ from site to site. If this energy difference is larger than the intersite hopping matrix element in the relevant Hamiltonian, then transitions will be strongly suppressed. Dephasing noise can come to the rescue here as it will lead to line broadening thus leading to increased overlap between sites without the loss of excitations from

the system (see lhs of Fig. 2). Alternatively, one may view dephasing noise as arising from the random fluctuations of energy levels. As a consequence, the fluctuating energy levels will occasionally come energetically close enough to allow fast excitation energy transfer between the sites (see rhs of Fig. 2). A moderate amount of fluctuations serves to enhance the transport while excessively strong fluctuations of the site energies will make the probability smaller for the sites to be energetically close. Hence we expect an optimal finite noise strength that maximizes transport between two sites. However,

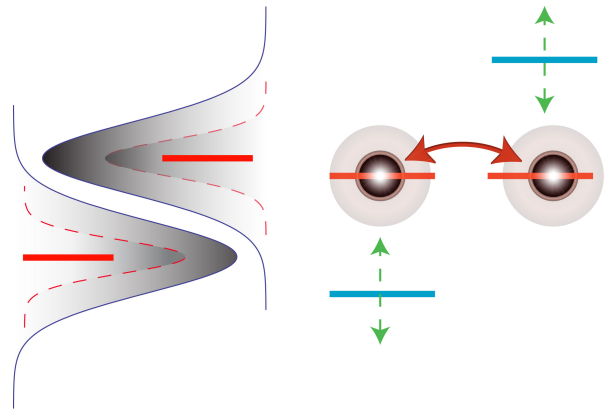


FIG. 1. Left: Local dephasing, for example due to random fluctuations of the energy levels, leads to line-broadening and hence increased overlap between sites. Right: Viewing these fluctuations dynamically, one finds that the energy gap between levels varies in time. The resulting nonlinear dependence of the transfer rate on the energy gap may therefore lead to an enhancement of the average transfer rate in the presence of dephasing noise.

the application of excessive noise and the concomitant reduction of the effective transition rate between sites can also be of advantage as it may effectively block unfavorable transfer paths from being followed [12].

2. Constructive & destructive interference

A quantum dynamical system may exhibit a wealth of constructive and destructive interference effects. The essential nature of this type of effect may be seen in the simple network depicted in Fig.2, where the coherent interaction is described by a Hamiltonian, $H = \sum_{k=1}^3 E_k |i\rangle \langle i| + \sum_{k=1}^2 J_{k3} (|k\rangle \langle 3| + h.c.)$, where $|i\rangle$ corresponds to an excitation in site i and we assume $J_{13} = J_{23}$. An excitation initially prepared in the antisymmetric state $|\psi\rangle = (|1\rangle - |2\rangle)/\sqrt{2}$ forms an eigenstate of this Hamiltonian which has zero overlap with the site 3 which we assume to be coupled dissipatively to a reaction center. Under natural conditions a pigment-protein complex is not normally excited in such an antisymmetric state, but will tend to receive a single excitation locally, for example on site 1.

The initial state localised on site 1 may of course be considered to be an equally weighted coherent superposition of the symmetric and the anti-symmetric states, i.e. $|1\rangle = [(|1\rangle - |2\rangle)/\sqrt{2} + (|1\rangle + |2\rangle)/\sqrt{2}]/\sqrt{2}$. Thanks to constructive interference the symmetric part of the initial state will propagate very rapidly into site 3, and from there into the reaction center, while the antisymmetric part will not evolve at all. Hence the transfer efficiency is limited to 50% in this situation. This trapping of population will be suppressed either via energetic disorder, which will release trapped population by inducing coherent oscillations between symmetric and anti-symmetric states, or by environmental dephasing noise which degrades interference effects and therefore destroys coherent trapping.

We note that these two mechanisms of noise-assisted transport are essentially independent of microscopic noises models, and could even be seen as highlighting the processes which noise sources *must* effect in order to drive efficient transport in networks where disorder and/or interference are important. The precise parameters and dynamical evolutions by which this is achieved by an environment *do* of course depend on the noise models and simulation techniques employed, but the physical mechanisms outlined above, which underlie the advantages and optimality of noise-assisted transport, are *not* qualitatively altered by any choice of model or approach. As a result, it is reasonable to illustrate the action of these mechanisms using fairly simple simulation tools, and in section II B we will demonstrate noise assisted transport using Lindblad master equations. This approach neglects several important factors, such as the effects of finite temperatures, but for the non-equilibrium conditions we shall consider, this approach yields results which both demonstrate the dramatic action of noise-assisted transport and which are also robust - at the same qualitative level of microscopic description as the proposed mechanisms - to changes in noise model.

Realistic systems require much more description, and simulations of experimental results certainly require more sophisticated models and simulation techniques. Our aim in this paper is to slowly build up a picture of the rich array of noise-driven processes which can lead to efficient energy transport, starting from the most basic ones described above and then incrementally adding additional details which lead to new mechanisms. As layers are added, so the methods employed will also become more involved. A good example of this is given in the next section, where we present a new principle of noise assisted transport which requires a consideration of two important properties of system-environment interactions which we have so far neglected in this article; the spectral density of environmental fluctuations and coherent vibronic couplings.

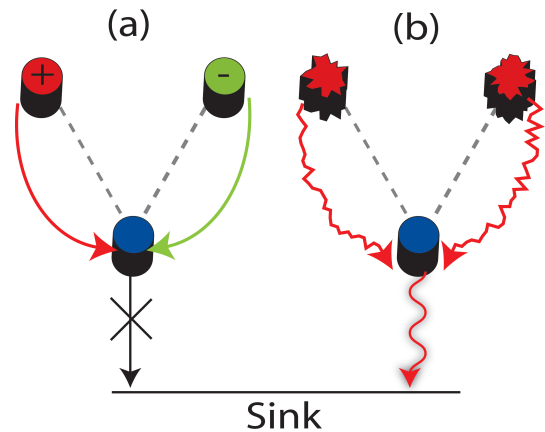


FIG. 2. A three-site network in which two sites 1 and 2 are each coupled to a third site 3 via an exchange interaction of the same strength. Site three is irreversibly connected to a sink. In (a) the excitation is delocalized over two sites (red and green) with equal probability of being found at either site but with a wave function that is antisymmetric with respect to the interchange of red and green. This state will not evolve due to destructive interference and hence no excitation will ever reach the reaction center. In (b) pure dephasing causes the loss of phase coherence and the two tunneling amplitudes no longer cancel, eventually leading to a complete excitation transfer to the sink.

3. Splitting energy levels - The phonon antenna

The presence of strong quantum coherent dynamics between energy levels can also allow an open system to optimize the efficiency of the energy transport. To this end, it should be noted that the energy levels of two sites that are coupled coherently will split, leading to new eigenstates of the global system, one of which is shifted upwards and one that is shifted downwards. As a consequence, one of the dressed energy levels may be moved closer to the desired final point of transport such as the reaction center. As the other level is moved upwards, a further process is required to drive its population towards the lower lying energy levels.

To this end, note that in this new basis dephasing noise will now induce transitions between these eigenstates (phase noise in the site basis becomes amplitude noise in the dressed basis) leading to energy transport towards the lower lying of the two energy levels. The transition rate between these two states will depend on temperature, the matrix element between these two eigenstates *and*, crucially, the spectral density at the energy difference between the two eigenstates. Matching the energy level splitting to the maximum of the spectral density of the environmental fluctuations can thus optimize energy transport. In this sense, we can argue that the two eigenstate of the coupled Hamiltonian harvest environmental noise to enhance excitation energy transport through the formation of a "phonon antenna".

As an illustrative example consider again the toy model

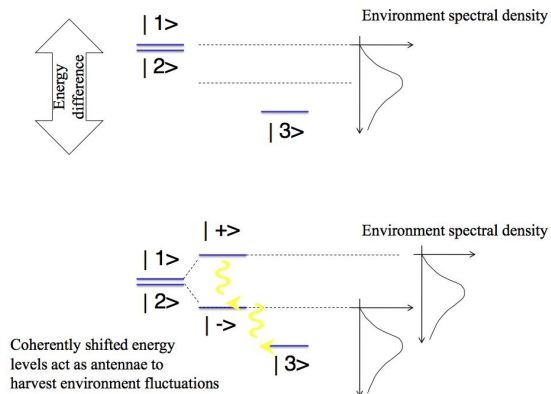


FIG. 3. In the upper half of the figure, two closely spaced energy levels are separated from a third level to which excitations should be delivered. A coherent interaction between the upper two energy levels leads to dressed states $|\pm\rangle$ with an energy splitting which, if matched to the maximum of the environment spectral density will optimize transport from the upper to the lower level. Hence the split levels act as an antennae for environmental fluctuations.

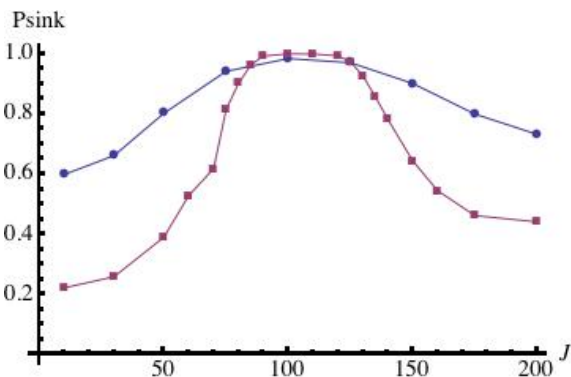


FIG. 4. Population transferred to sink at $t = 5\text{ps}$ as a function of J_{12} for a Lorentzian spectral density with FWHM of 50cm^{-1} (blue dots) and 10cm^{-1} (purple squares). Numerical results obtained using secular Bloch-Redfield equations. For all curves $J_{23} = 30\text{cm}^{-1}$ and the environment temperature is 77K .

consisting in a three site network where site 3 is coupled to a reaction center and let us assume that a Lorentzian spectral density that is peaked at 200cm^{-1} (which is typical for FMO) and a FWHM of around 50cm^{-1} (which is narrower than estimated for the FMO). Setting the energy of site 1 and 2 to $\epsilon_1 = \epsilon_2 = 300\text{cm}^{-1}$ and $\epsilon_3 = 0\text{cm}^{-1}$, it then turns out that the transfer will be optimized for a coupling J_{12} between sites 1 and 2 of around $J_{12} = 100\text{cm}^{-1}$ which results in a splitting of $\Delta E = 200\text{cm}^{-1}$. Figure 4 shows the population transferred to a sink P_{sink} connected to site 3 after 5 ps of evolution described by a standard secular Bloch-Redfield master equation and the Lorentzian spectral function de-

scribed above. The transfer to the sink was described by a Lindbladian with a transfer rate of 1ps^{-1} , $J_{13} = 0$, $J_{23} = 30\text{cm}^{-1}$ and the bath temperature was taken as 77K . A clear maximum is seen for $J_{12} = 100\text{cm}^{-1}$ which can be interpreted as a result of the phonon antenna effect set out in Fig. 3. Figure 4 also shows results for a narrower Lorentzian (FWHM 10cm^{-1}), showing that the enhancement at $J = 100\text{cm}^{-1}$ is much more strongly peaked as one would expect. These results suggest that exciton couplings might be used to exploit the structure of the noise spectrum of the protein surroundings, and that the advantages of doing this increase as the structure of the environmental spectral function becomes sharper.

However, when the structure of the spectral function contains very sharp resonances, the resonant modes can no longer be treated with standard master equation approaches. The derivation of most master equations from microscopic system-bath Hamiltonians normally relies on the fact that the environment contains an extremely large number of modes and that the coupling to any individual mode is weak. However, a spectral function that is very sharply peaked at some characteristic frequency ω implies a strong coupling to a discrete mode of the environment, and such an interaction can induce a significant *coherent* modification of the exciton dynamics while the mode is driven strongly out of equilibrium by the exciton dynamics. These discrete mode effects were explored using a recently-developed time-adaptive renormalisation group technique that allows strong interactions to discrete modes to be treated as part of an environment with an arbitrary residual spectral density [16]. This method produces numerically exact results with controllable errors, and it was found that discrete modes may *coherently* modulate population dynamics over ps timescales whilst the continuous part of the spectral density drives efficient population transfer [16, 17].

Another approach to this problem is to consider the strong coupling to a discrete mode as part of the system and then to treat the residual smooth parts of the spectral density as the environment. This approach requires a large expansion of the Hilbert space of the effective exciton-mode system and makes simulations considerably more complex, especially if the residual bath has a non-Markovian character. This approach is thus only suitable for simple systems with relatively simple residual spectral densities, but it is very useful for illustrating the elementary concepts of strong exciton-mode interactions. We now consider such a model using the Hamiltonian given by Eq. (2) to describe three sites, as described above, in which each site is coupled coherently to a single harmonic oscillator of frequency $\omega = 200\text{cm}^{-1}$ and coupling constant $g_i = 30\text{cm}^{-1}$. To clearly demonstrate the discrete phonon antenna effect, we neglect background dephasing here, but this will be treated in detail in a forthcoming work [18]. The simulations are performed using exact diagonalisation and the simulation results were found to converge with 4 bosonic levels per mode.

Figure 5 shows the population in the sink as a func-

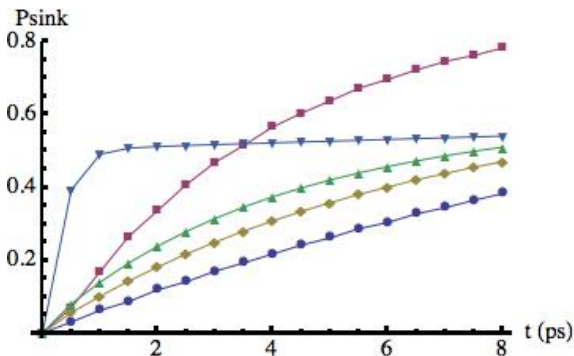


FIG. 5. P_{sink} as a function of time for three-site system, where each site is coupled to a mode of frequency 200cm^{-1} with coupling strength $g = 30\text{cm}^{-1}$. A strong enhancement of transport is seen for $J_{12} = 100\text{cm}^{-1}$ (squares). The other curves are $J_{12} = 150\text{cm}^{-1}$ (diamonds), $J_{12} = 200\text{cm}^{-1}$ (triangles), $J_{12} = 300\text{cm}^{-1}$ (inverted squares) and $J_{12} = 50\text{cm}^{-1}$ (dots). For all curves $J_{23} = 30\text{cm}^{-1}$ and the initial state of the vibrational mode is a thermal state at 77 K.

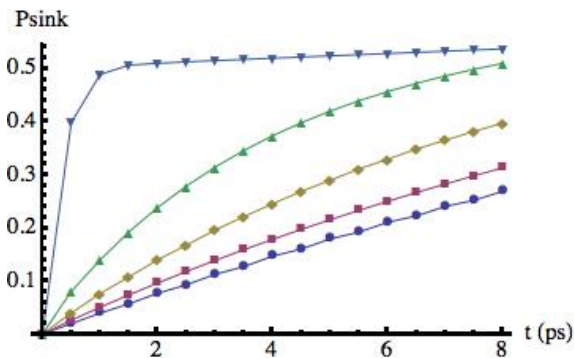


FIG. 6. P_{sink} as a function of time for a three-site system without any coupling to a mode. Weak transport is now seen for $J_{12} = 100\text{cm}^{-1}$ (squares). The other curves are $J_{12} = 150\text{cm}^{-1}$ (diamonds), $J_{12} = 200\text{cm}^{-1}$ (triangles), $J_{12} = 300\text{cm}^{-1}$ (inverted squares) and $J_{12} = 50\text{cm}^{-1}$ (dots). For all curves $J_{23} = 30\text{cm}^{-1}$ and the initial state of the vibrational mode is a thermal state at 77 K.

tion of time for a range of J_{12} values. It can be seen that the behaviour of P_{sink} is strongly non-monotonic with a large enhancement of the population transport when $J_{12} = 100\text{cm}^{-1}$. For these values the hybrid states $|\pm\rangle$ are resonant with the vibration sidebands of each site (see Fig. 7) and the mode-exciton interaction mediates strong transitions between sites by allowing efficient coherent tunneling between the degenerate vibrationally excited states of the electronic excitations. For other values of J_{12} the $|\pm\rangle$ states are detuned from the mode sidebands and vibration-mediated transport is dramatically reduced. Note also that for $J_{12} = 300\text{cm}^{-1}$ the lower state $|-\rangle$ is resonant with site 3. This leads to a rapid transport of 50% of the population, but the 50% initially held in the $|+\rangle$ state is at such a high energy that it cannot transfer population to the sink via site 3

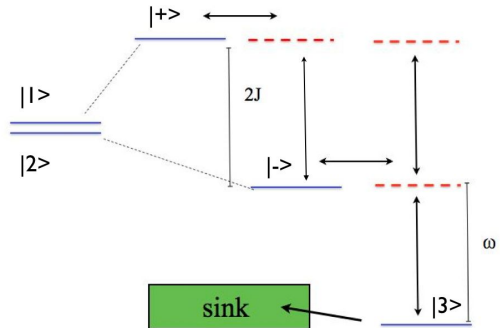


FIG. 7. Energy level scheme for three-site and sink system (blue lines) showing vibrational sideband levels (dashed red lines). The coupling J_{12} splits the degenerate transitions, forming new super position states $|\pm\rangle$, and can bring these electronic levels into resonance with the sidband structure. Under these conditions fast, coherent inter-site transport (black arrows) becomes possible through the new exciton-mode energy level landscape.

in the absence of background noise.

Figure 6 shows results for the same parameters in the absence of the mode. One now observes a monotonic behaviour of the transport rates as J_{12} is increased, and by comparison with Fig. 5, the dramatic resonant enhancement of transport observed at $J_{12} = 100\text{cm}^{-1}$ is highlighted. These results suggest that tuning of excitonic couplings to "harvest" the available noise spectrum is most effective when the quasi-discrete features are exploited. It is in this sense - just as excitonic interactions allow chromophores to sample larger parts of the optical spectrum - that we refer to such coherent sampling of discrete features or maxima of the spectral function as the phonon antennae effect. Not only do these allow for tremendous gains in transport efficiency, their strong quantum mechanical interaction with the exciton appears to strongly modify the behaviour and lifetime of coherence dynamics (not shown).

B. The principles at work: FMO and LHII

Here we will briefly analyse how these principles are put to work to explain aspects of noise assisted transport in two different pigment-protein complexes.

1. The FMO complex

To illustrate how the general principles outlined in the previous section may feature in a realistic scenario, we will consider the example of excitation transfer across a monomer of the FMO complex, which can be modeled as a 7 sites network and for which detailed information

concerning the system Hamiltonian is available [19]. We ignore here the recent addition of an eighth site [20] as it does not affect the general arguments and was unlikely to have been present in recent experiments reported in [3, 5].

Given the strong coupling of sites 1 and 2, these levels are shifted and mixed and the dynamics is conveniently described using a hybrid basis [12] for these two sites that we denote by $|\pm\rangle$. In this basis, the Hamiltonian has the local site energies and coupling structure shown in Figure 8a, where site 3 is connected to a sink node from which excitation is transferred to the reaction center and all the remaining sites have been packed in a block (labeled as "additional sites" in Figure 2) that is uncoupled from the level $|+\rangle$.

When an excitation is injected in site 1, the coherent evolution leads to transfer efficiency P_{sink} below 60%, far from the ideal transfer, represented in Fig. 8 by the red horizontal line. The *coherent interaction* between sites 1 and 2 leads to level splitting and moves one of these energetically closer to site 3 while the other is farther removed. The introduction of dephasing noise with a given spectral density can dramatically add to this picture and lead to perfectly efficient transport to the sink, as illustrated in the part (b) of Fig. 8. Environmental fluctuations lead to transitions between states $|+\rangle$ and $|-\rangle$ and the resulting transition rate will depend on the spectral density at the level splitting of the dressed states $|+\rangle$ and $|-\rangle$. Indeed, inspection of the relevant Hamiltonian reveals that the coupling between sites 1 and 2 is of the order of 93cm^{-1} and leads to a splitting between the dressed states $|+\rangle$ and $|-\rangle$ of very close to 200cm^{-1} which matches the maximum of the spectral density of the environmental fluctuations used in [19]. It is hence tempting to speculate that nature has optimized the intersite coupling and/or spectral density to provide a perfect match between the maximum of the spectral density and the level splitting of the dressed states $|+\rangle$ and $|-\rangle$ thus exploiting the idea that quantum coherent interaction support an "antenna for phonons".

Furthermore, coherent oscillations between level $|-\rangle$ and the rest of the complex are now largely suppressed (due to noise and destructive interference), while an incoherent transfer path between previously decoupled levels $|\pm\rangle$ is now active, leading to a fast transfer of population to the sink via $|-\rangle$. Within this model, it is possible to optimize the local dephasing rates so as to reproduce the observed transfer rates in the correct time scale. More detailed discussions can be found in the literature [6, 7, 10, 12].

Recent molecular dynamics simulations have also shown that the spectral density of pigment-protein complexes such as the FMO complex contain a large number of sharp features which could be exploited via the mechanism described above [21–23]. Moreover, spectral hole burning and fluorescence line narrowing experiments have also shown that a number of modes with frequencies comparable to the energy differences between excitons

couple strongly to the electronic degrees of freedom in the FMO complex [24–26]. Given that vibration-mediated tunneling is also implicated in a range of other important biological transport processes, such as olfaction [27], it does not seem unreasonable that EET dynamics in pigment-protein complexes could take advantage of the rich spectral structure of their local environments by appropriately tuning the inter-site interactions to sample the maxima of the spectral function.

Indeed, it has also been shown in [12] that a discrete mode coupled to each site in the FMO complex could also induce efficient transport, and in some cases could even outperform the optimised, purely incoherent noise assisted transport which arises from a Lindblad treatment of the environment. Given the observed presence of a wide range of discrete features in the phonon spectrum of FMO, it is likely that both incoherent and discrete phonon antenna effects could play a role in the efficient energy transport seen in experiments, with the latter mechanism possibly contributing to enhanced, longer-lasting coherent dynamics, as observed in [12]. A full analysis of the dynamics of FMO in the presence of both discrete modes and continuous spectral densities with maxima close to exciton energies differences will be appear in [28].

2. The LHII complex

Here we consider the LHII complex from the photosynthetic unit of purple bacteria [29]. The photosynthetic unit is composed of a membrane that contains only two types of antennae complexes, LHI and LHII. The former are believed to form ring-like structures that enclose the reaction center while the latter transfer energy to the reaction center via the LHI antennae. The LHII antennae consists of two subunits, the B800 and the B850 ring. The B800 ring, absorbing around 800nm, consists of nine pigments, which have their molecular plane arranged perpendicular to the symmetry axis. The B850 ring, absorbing around 850nm, consists of nine repeating pairs of α - β pigments, with opposite transition dipole moments and their molecular planes parallel to the symmetry axis.

Here we make the simplifying assumption that the interaction between pigments is well approximated by a dipole-dipole interaction of the form

$$V_{ij} = \frac{1}{4\pi\epsilon|\vec{r}_{ij}|^3} \left[\vec{\mu}_i\vec{\mu}_j - 3(\vec{\mu}_i\hat{r}_{ij})(\vec{\mu}_j\hat{r}_{ij}) \right] \quad (1)$$

where $\vec{r}_{ij} = \vec{r}_i - \vec{r}_j$ is the vector joining pigment i with pigment j and \hat{r}_{ij} is the corresponding unit vector. We chose $\epsilon = 1.3 \cdot 8.8510^{-12} \text{C}^2/\text{Nm}^2$. The dipole moments are assumed to be of equal modulus $|\vec{\mu}| = 2.046 \times 10^{(-29)} \text{Cm}$. The dipole moments are nearly perpendicular to the symmetry axis and to the radial direction (see [30] for details).

With this information it is possible to determine the interaction strengths between any pair of pigments. In

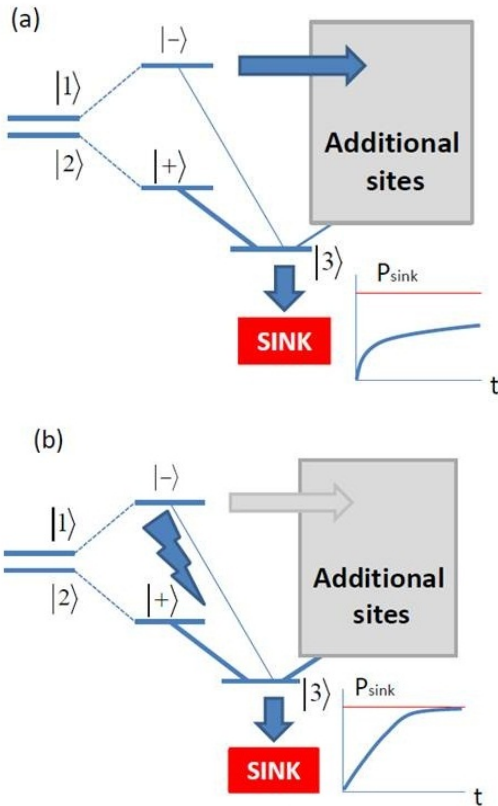


FIG. 8. Noise-assisted energy transfer across FMO can be qualitatively understood by introducing a hybrid basis of local sites. While a purely unitary evolution yields to inefficient transport, as discussed in the text, the presence of dephasing noise eliminates inefficient transport paths while opening up new channels for excitation transfer. While the estimation for the transfer efficiency under coherent evolution is well below 100%, a simple noise model brings this number close to perfect efficiency within the observed transfer time.

the B800 ring neighboring pigments experience an interaction strength of around -26.7cm^{-1} while in the B850 ring neighboring pigments within a $\alpha\text{-}\beta$ pair experience an interaction of about 190.8cm^{-1} and between neighboring pairs of 239.4cm^{-1} while the coupling from B800 to B850 between the closest pigments is of the order of 12cm^{-1} . Employing these parameters it is now straightforward to observe that the transfer from the B800 to the B850 benefits from the presence of dephasing noise. Fig 9 shows the non-monotonic dependence of the transfer rate between the two rings versus the noise strength under the assumption that all pigments are subject to noise of identical strength. Here the noise assists in bridging the energy gap between the B800 and the B850 ring. Strong noise does however tend to suppress delocalization of excitons in each ring and thus suppress coherent superpositions that may lead to enhanced transport from B800 to B850.

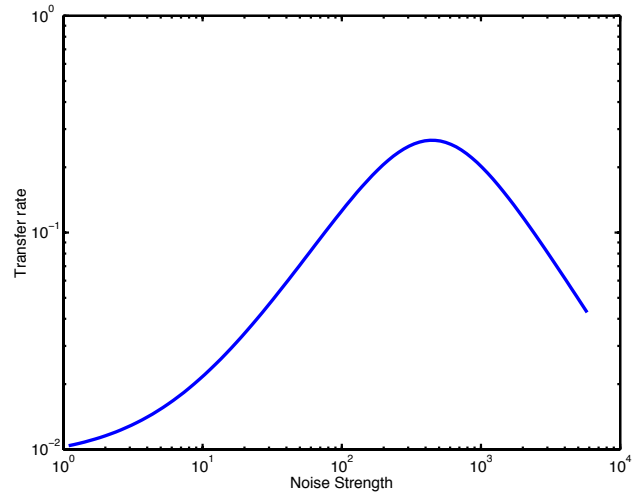


FIG. 9. The B800-B850 transfer rate versus the noise strength exhibiting a non-monotonic behaviour in the noise strength.

III. REFLECTIONS ON THE MICROSCOPIC ORIGIN OF LONG-LIVED COHERENCE

Having given an overview of the key concepts underpinning noise-assisted transport, we proceed with our general discussion of the role of noise in PPC dynamics by going a little more into the details of the microscopic couplings which generate the essential processes of pure dephasing (destruction of interferences) and exciton relaxation. Without leaping into major simulations, we aim to point out a number of effects which might be observable in experiments, and which could potentially help us to pinpoint the physics behind a number of currently ill-understood observations that have been made in experiments and ab initio simulations.

Let us consider the following standard Hamiltonian of chromophores which are linearly coupled to protein fluctuations in their excited states. Defining bosonic annihilation and creation operators a_{ki} , a_{ki}^\dagger for the independent, uncorrelated fluctuations of frequency ω_k of the protein environments acting on site i , and denoting an optical excitation on site i by the state $|i\rangle$, the Hamiltonian for a single excitation can be written as,

$$H = \sum_i ((\epsilon_i + X_i)|i\rangle\langle i| + H_i^B) + \sum_{i \neq j} J_{ij}|i\rangle\langle j|, \quad (2)$$

where $X_i = \sum_k g_{ik}(a_{ki} + a_{ki}^\dagger)$ and $H_i^B = \sum_k \omega_k a_{ki}^\dagger a_{ki}$, where ω_k are the frequencies of the protein fluctuations and g_{ik} their coupling strength to state $|i\rangle$ ($\hbar = 1$ throughout). Assuming identical environments for each site, the dissipative effect of the environment on the excitons is fully-characterised by the spectral density of the environment $G(\omega) = \sum_k g_{ik}^2 \delta(\omega - \omega_k)$, which we discussed extensively in the previous section. It is normally taken that the electronic couplings J_{ij} between

sites is stronger than the pigment-protein interaction and that the appropriate basis for analysing experimental results corresponds to that of the excitonic eigenstates $|e_n\rangle = \sum_i C_i^n |i\rangle$.

Rewriting the Hamiltonian in the exciton basis, we obtain,

$$\begin{aligned}
H &= \sum_n E_n |e_n\rangle \langle e_n| + \sum_n Q_n |e_n\rangle \langle e_n| \\
&+ \sum_{n \neq m} (R_{nm} |e_n\rangle \langle e_m| + R_{nm}^\dagger |e_m\rangle \langle e_n|) \\
&+ \sum_i H_i^B. \tag{3}
\end{aligned}$$

The new couplings to the bath are given by $Q_n = \sum_{k,i} g_{ik} |C_i^n|^2 (a_{ki} + a_{ki}^\dagger)$ and $R_{nm} = \sum_{k,i} g_{ik} C_i^n C_i^m (a_{ki} + a_{ki}^\dagger)$. As was mentioned in the introduction, in this basis the exciton states, which is the appropriate basis for weak system environment coupling, are stationary under the action of the electronic Hamiltonian and dynamics arise solely through the action of the bath couplings on the system. From Eq. (3) one can see that these interactions come in two distinct flavours, namely inter-exciton (transverse) transfer terms ($\propto R_{nm}$) and diagonal (longitudinal) fluctuations of the exciton energies ($\propto Q_n$). During the evolution of an initially-prepared superposition of exciton states, the total dephasing time of the superposition roughly contains two contributions, a relaxation part coming from transverse processes and a pure dephasing part coming from the longitudinal processes.

Before going on to discuss the case of uncorrelated fluctuations, we briefly present the parameters

$$\gamma_{nm} = \sum_{i,j} C_i^n C_i^m C_j^n C_j^m e^{-r_{ij}/r_c}, \tag{4}$$

$$\begin{aligned}
a_{nm} &= \sum_{i,j} ((C_i^m)^2 (C_j^m)^2 + (C_i^n)^2 (C_j^n)^2 \\
&- 2(C_i^m)^2 (C_j^n)^2) e^{-r_{ij}/r_c}, \tag{5}
\end{aligned}$$

where r_c is the correlation length of the fluctuations at each site and r_{ij} are the inter-pigment distances [19]. The off-diagonal quantities γ_{nm} are proportional to the strength of the transition rates between excitons n and m in Bloch-Redfield theory, and pure-dephasing processes between excitons n and m in modified Redfield theory are proportional to a_{nm} [19]. Although we will not discuss spatial correlations explicitly, we note that when r_c is much larger than the size of the complex $\gamma_{nm} \approx |\langle e_n | e_m \rangle|^2$, $a_{nm} \approx 0$ and the *total* (transverse and longitudinal) coupling to the bath *vanishes* in the one-excitation manifold. Spatial correlations thus reduce dephasing *and* transport rates by roughly similar amounts.

Returning to uncorrelated environments, it is well known that delocalisation of the excitons over extended regions of roughly N sites leads to a $1/N$ suppression of the pure-dephasing of ground state-excited state coherences via the phenomena of *motional narrowing* [31].

However, due to disorder the delocalisation length in typical PPCs is often restricted to only a few sites, and indeed several PPCs *only* contain a few sites in total. Nevertheless, even if the excitons are only delocalised over two sites, a significant suppression of zero-quantum coherence dephasing can arise if the electronic wavefunctions are nearly equally distributed over the two sites, i.e. the eigenstates are symmetric and anti-symmetric combination of the two local excitation states. To see this clearly, imagine we have a dimer system in which $\epsilon_1 - \epsilon_2 \ll J$. The two excitonic states are then $|e_\pm\rangle = (|1\rangle \pm |2\rangle)/\sqrt{2}$. In the exciton basis the exciton-phonon Hamiltonian becomes,

$$\begin{aligned}
H &= \sum_{n=+,-} E_n |e_n\rangle \langle e_n| + \frac{1}{2} Q_n \underbrace{\left(|e_+\rangle \langle e_+| + |e_-\rangle \langle e_-| \right)}_{=i.d} \\
&+ (R_{+-} |e_+\rangle \langle e_-| + \text{h.c.}) + \sum_n H_n^B. \tag{6}
\end{aligned}$$

As indicated by the underbrace, the longitudinal coupling to the excitons vanishes (in the one-excitation sector) when the eigenstates are symmetric/anti-symmetric combinations. The bath-induced dynamics now proceeds purely through transverse terms and dephasing only arises through relaxation. We shall refer to this case as *relaxation-limited dephasing*. In general, if the excitons are delocalised over N sites and excitonic couplings are very strong, then the eigenstates are of the form $|\tilde{e}_n\rangle = \sum_{k=1}^N e^{-ink/N} |i\rangle$ and will also not be subject to any longitudinal bath coupling.

Our discussion in this section has so far made no assumptions about the spectral function of the environment, but in order to illustrate a few ideas we will now consider the case of a sufficiently weak exciton-phonon coupling where the influence of the bath can be treated in a Markovian (Redfield) approximation. In this limit, one can rigorously define the relaxation time T_1 , the total dephasing time of coherences T_2 and the pure-dephasing time T_2^* . The three times are related by $1/T_2 = 1/2T_1 + 1/T_2^*$. The relaxation time T_1^{-1} describes the rate of population transfer induced by the transverse couplings in Eq. (3) and T_2^* arises from longitudinal terms. In the limit of relaxation-limited dephasing, where T_2^* diverges, $T_2 = 2T_1$ and the dephasing rate is actually *slower* than the population transfer rate. However, in most experiments performed in liquids and the solid state, $T_2 \ll T_1$ due to the dominant contribution of pure dephasing terms. This is often also true in realisations of qubits in quantum information science, and removal of these processes is currently a topic of major research.

In current 2D spectroscopy experiments it is often possible to measure the population lifetimes (giving an estimate of T_1) and the total dephasing time (T_2) of coherences separately. By comparing these numbers, the

extent of pure dephasing can be inferred and the extent of the suppression of pure-dephasing terms by delocalisation might also be extracted. This might possibly allow strongly-coupled excitonic states to be identified and could also thereby provide a consistency-check of Hamiltonians and dynamical models which have been proposed for these systems. From this point of view, it must be noted that non-Markovian dynamics are thought to play an important role in PPCs such as FMO [32], and in these cases there is no simple relation between the typical timescales associated with pure dephasing, relaxation and the total dephasing timescale(s). However, non-perturbative simulation techniques can address this, and this will be dealt with in a forthcoming work [28].

One example of this effect could be found by looking at excitons associated with sites 1 and 2 of FMO. In most published Hamiltonians the difference between local excitation energies of sites 1 and 2 are smaller than the large excitonic coupling between them, and two exciton states contain strong contributions from symmetric and anti-symmetric combinations of sites 1 and 2. Within the model and modified Bloch-Redfield approximation presented by Adolphs and Renger [19], the coherence ρ_{nm} between excitons n and m decoheres under pure dephasing processes as $\rho_{nm} \propto e^{-a_{mn}(g(t)-g(0))}$ (we have neglected the relaxation-induced contribution to the decoherence). The coherence between exciton n and the ground state ρ_{gn} similarly decoheres as $\rho_{gn} \propto e^{-\gamma_{nn}(g(t)-g(0))}$. In both cases, the spectral density-dependent functions $g(t)$ are the same [19]. The relative strengths of the pure dephasing dynamics of the inter-exciton and ground-exciton can be therefore be estimated by looking at the ratios a_{nm}/γ_{nn} or a_{nm}/γ_{mm} , which are independent of the spectral function. Lower and upper estimates of these ratios were obtained by computing a_{nm}, γ_{nn} and γ_{mm} for the excitons $|e_n\rangle, |e_m\rangle$ of FMO Hamiltonians with the largest contributions from sites 1 and 2. Assuming uncorrelated environments, we found that $a_{nm}/\gamma_{nn} \approx a_{nm}/\gamma_{mm} \approx 10^{-1} - 10^{-3}$, with the lower bound being obtained from the Hamiltonian of Adolphs and Renger [19] and the upper bound from the Hamiltonian presented in [33]. The large suppression of the inter-exciton pure dephasing contribution at the upper bound, would most likely lead to a relaxation-limited dephasing.

After completion of this work, an explicit example of relaxation-limited dephasing has also been given in [34]. They have computed the dynamics for site population dynamics of sites 1 and 2 of the FMO complex using a weak coupling non-interaction blip approximation (NIBA) developed in the context of the spin-boson problem [35]. Pachon and Brumer [34] point out for the parameters of these sites, the small site energy difference and large excitonic coupling leads to a suppression of pure-dephasing contributions to the total dephasing rate, and at 77 K, the dephasing rate they predict is indeed close to the relaxation-limited case $T_2 \approx 2T_1$. However, as we stress above, this relaxation-limiting suppression of

pure-dephasing - which does not rely on a non-Markovian treatment of the system-bath interactions, is only relevant under conditions where site energies differences are much smaller than inter-site couplings. In the FMO complex experiments, the long-lasting excitonic coherences are observed between the two lowest energy excitons, which correspond to sites 3 and 4, rather than sites 1 and 2. These sites have energy differences and couplings of roughly equal magnitude [19], or much greater site energy differences [33]. While relaxation-limited dephasing can play a role for certain pathways in the FMO dynamics, it is unlikely to provide a *general* explanation for the most significant long-lasting coherences observed in FMO, as is claimed in [34]. It should also be pointed out that the long-lasting inter-exciton (not to be confused with inter-site) coherences at 77 K in FMO persist for approximately 1.8 ps, much longer than those predicted in [34].

It is important to also note that the long-lasting coherences found in [34] are not due to any non-markovian effects; the use of the NIBA approach (which may not be reliable in the relevant parameter regime, see footnote [36] gives non-perturbative *renormalisation* of the parameters which determine the relaxation and dephasing rates, but the dynamics themselves are simple, strictly exponentially-damped oscillations and the coherence lifetimes could be predicted from polaron perturbation theory. This, and the agreement of this theory with numerical simulations, could also suggest that for the simple Ohmic spectral density and weak-coupling parameters used in the literature, advanced simulation techniques are not required for complexes such as FMO, though a comprehensive understanding of EET dynamics is still lacking as it is unlikely that the simple Ohmic spectral density describes all aspects of the system-bath physics.

One of our reasons for discussing delocalisation-induced suppression of pure-dephasing is that the interexciton coherences in FMO appear to dephase much more slowly (~ 1 ps) than the typical ($\sim 70 - 150$ fs) dephasing times of the ground-exciton coherences between excited and ground states [5]. If the dephasing of ground-exciton coherences comes from the same set of fluctuations, one would expect roughly similar pure-dephasing times for the zero-quantum coherences as well. One potential solution is that the fluctuations are *spatially correlated*, and has been used to analyse the results of a number of experiments on PPCs and conjugated polymers [37, 38]. However, a number of recent quantum chemistry and molecular dynamics simulations of the FMO protein have, somewhat inconveniently, found no evidence for significant spatial correlations between different pigments [21–23].

An alternative possibility that may be appropriate for excitons which are strongly delocalised over a few sites in PPCs is suggested by relaxation-limited dephasing. We have shown that strong excitonic coupling can suppress pure dephasing amongst excitons in the one-excitation sector, but when the electronic ground state

$|g\rangle$ is also included in the Hamiltonian, it can be seen that the excitons are no longer protected from the longitudinal terms if they are in a state that spans excitation number sectors e.g. a ground-exciton coherence $|e_n\rangle\langle g|$. This means that a ground-exciton coherence will feel a motionally-narrowed, but still potentially large pure dephasing, whereas an inter-exciton coherence between $|e_{\pm}\rangle$ -like states will not be subject to this pure dephasing at all.

It is important to notice that, unlike spatial correlations which lead to a dynamical decoupling of the entire exciton-phonon interaction, the relaxation-limited case corresponds to the entire weight of the exciton-phonon coupling being transferred to the inter-exciton couplings. In this sense, and under appropriate conditions, coherences are protected without effecting transport efficiency. The inter-exciton coherence dephasing time is now essentially determined by the lifetimes of excitons, and has a much stronger, and thus tunable, dependence on the exciton energy differences compared to pure dephasing which is frequency-independent. For example, the Redfield relaxation rate Γ_{+-} between excitons $+$ and $-$ is given by [19],

$$\Gamma_{+-} = \pi[(1 + n(E_{+-}))G(E_{+-}) + n(E_{-+})G(E_{-+})], \quad (7)$$

where $E_{nm} = E_n - E_m$, E_n is the energy of the n th exciton and $n(\omega)$ is the thermal bosonic occupation of a mode with frequency ω . The total dephasing time of an inter-exciton coherence can be significantly longer than the ground-exciton dephasing time in the relaxation-limited case when the exciton lifetimes determined from Eq. (7) are smaller than the ground-exciton dephasing rate. For our dimer example, when $\delta E_{\pm} \approx 2J$ is much larger than the maximum of $G(\omega)$, the lifetimes of the states will be long because $\Gamma_{nm} \propto G(E_{nm})$. The essential point here is that relaxation and pure-dephasing are determined by very different regions *and* properties of the spectral function, with pure dephasing rates at long times being very sensitive to the *functional form* of $\lim_{\omega \rightarrow 0} G(\omega) \coth(\beta\omega/2)/\omega^2$ [39]. Therefore for transitions between states separated by large energy differences, relaxation-limited dephasing may significantly increase the effective inter-exciton dephasing time compared to the ground-exciton dephasing rates, this the

difference depending sensitively on the spectral density used.

The mechanism described above is another example of how excitonic interactions can be used to shift the dominant effects of the environment between spectral features - here removing effects of aggressive low frequency dephasing fluctuations - and conceptually allowing lifetimes and coherence times on the same order of magnitude as each other and the transport time (which is controlled by the lifetimes). This could be an important *part*, though certainly not the only mechanism, of the physics underlying long-lasting coherences. However, the question of *why* these systems might choose to do these things - especially the preservation of coherences - remains as elusive as ever.

We finally note that this idea of electronic protection of inter-exciton coherences could be tested in dimer systems with strong excitonic interactions such as those found in reaction centers, and a detailed theory of the ideas presented in the last two sections of this article will appear shortly [28].

IV. CONCLUSIONS

In this work we have summarized recent work concerning several aspects of the dynamics of quantum networks in contact with environments such as pigment-protein complexes. We have discussed the basic principles underlying the dynamics of such systems and formulated the concept of efficient transport mediated by phonon antennae induced by coherent dynamics. We also discussed the possible relevance of motional narrowing on the unexpectedly long lifetime of zero coherences in pigment-protein complexes such as FMO. A more detailed account of these two aspects will be published elsewhere.

ACKNOWLEDGMENTS

This work was supported by the Alexander von Humboldt-Foundation, the EU STREP project CORNER and the EU Integrated Project Q-ESSENCE. Aspects of this work have benefitted from discussions with J. Cai, F. Caruso, F. Caycedo-Soler, J. Prior, A. Datta, and G.S. Engel.

-
- [1] Plenio, M.B. & Virmani, S. 2007 An introduction to entanglement measures. *Quant. Inf. Comp.* **7**, 1.
 [2] Mukamel, S. 2010 Signatures of quasiparticle entanglement in multidimensional nonlinear optical spectroscopy of aggregates. *J. Chem. Phys.* **132**, 241105.
 [3] Engel, G.S., Calhoun, T.R., Read, E.L., Ahn, T.K., Manical, T., Cheng, Y.C., Blankenship, R.E. & Fleming, G.R. 2007 Evidence for wavelike energy transfer through quantum coherence in photosynthetic systems. *Nature* **446**,

782 – 786.

- [4] Mercer, I.P., El-Taha, Y.C., Kajumba, N., Marangos, J.P., Tisch, J.W.G., Gabrielsen, M., Cogdell, R.J., Springate, E., Turcu, E. 2009 Instantaneous mapping of coherently coupled electronic transitions and energy transfers in a photosynthetic complex using angle-resolved coherent optical wave-mixing. *Phys. Rev. Lett.* **102**, 057402.

- [5] Panitchayangkoon, G., Hayes, D., Fransted, K.A., Caram, J.R., Harel, E., Wen, J.Z., Blankenship, R.E. & Engel, G.S. 2010 Long-lived quantum coherence in photosynthetic complexes at physiological temperature. *Proceedings of the National Academy of Sciences of the United States of America* **107**, 12766 – 12770.
- [6] Mohseni, M., Rebentrost, P., Lloyd, S. & Aspuru-Guzik, A. 2008 Environment-assisted quantum walks in photosynthetic energy transfer. *Journal of Chemical Physics* **129**, 174106.
- [7] Plenio, M.B. & Huelga, S.F. 2008 Dephasing-assisted transport: quantum networks and biomolecules. *New Journal of Physics* **10**, 113019.
- [8] Cho, M., Vaswami, H.M., Brixner, T., Stenger, J. & Fleming, G.R. 2005 Exciton analysis in 2D electronic spectroscopy. *J. Phys. Chem. B* **109**, 10542.
- [9] Olaya-Castro, A., Lee, C.F., Olsen, F.F., & Johnson, N.F. 2008 Efficiency of energy transfer in a light-harvesting system under quantum coherence. *Phys. Rev. B* **78**, 085115.
- [10] Caruso, F., Chin, A.W., Datta, A., Huelga, S.F. & Plenio, M.B. 2009 Highly efficient energy excitation transfer in light-harvesting complexes: The fundamental role of noise-assisted transport. *Journal of Chemical Physics* **131**, 105106.
- [11] Rebentrost, P., Mohseni, M., Kassal, I., Lloyd, S., & Aspuru-Guzik, A. 2009 Environment-Assisted Quantum Transport. *New Journal of Physics* **11**, 033003.
- [12] Chin, A.W., Datta, A., Caruso, F., Huelga, S.F. & Plenio, M.B. 2010 Noise-assisted energy transfer in quantum networks and light-harvesting complexes. *New Journal of Physics* **12**, 065002.
- [13] Caruso, F., Chin, A.W., Datta, A., Huelga, S.F. & Plenio, M.B. 2010 Entanglement and entangling power of the dynamics in light-harvesting complex *Phys. Rev. A* **81**, 062346.
- [14] Huelga, S.F. & Plenio, M.B. 2011 Quantum dynamics of bio-molecular systems in noisy environments. *Procedia Chemistry* **3**, 248.
- [15] Caruso, F., Montangero, S., Calarco, T., Huelga, S.F. & Plenio, M.B. 2011 Coherent open-loop optimal control of light-harvesting dynamics. *arXiv:1103.0929*.
- [16] Prior, J., Chin, A.W., Huelga, S.F. & Plenio, M.B. 2010 Efficient simulation of strong system-environment interactions *Phys. Rev. Lett.* **105**, 050404.
- [17] Chin, A.W., Rivas, A., Huelga, S.F., & Plenio, M.B. 2010 Exact mapping between system-reservoir quantum models and semi-infinite discrete chains using orthogonal polynomials. *J. Math. Phys.* **51**, 092109.
- [18] del Rey, M., Chin, A.W., Huelga, S.F. & Plenio, M.B. 2012 In preparation.
- [19] Adolphs, J., & Renger, T. 2006 How Proteins Trigger Excitation Energy Transfer in the FMO Complex of Green Sulfur Bacteria. *Biophys. J.* **91**, 2778.
- [20] Schmidt am Busch, M., Müh, F., El-Amine Madjet, M., & Renger, T. 2011 The Eighth Bacteriochlorophyll Completes the Excitation Energy Funnel in the FMO Protein. *J. Phys. Chem. Lett.* **2**, 93 – 98.
- [21] Shim, S., Rebentrost, P., Valleau, S. & Aspuru-Guzik, A. 2011 Microscopic origin of the long-lived quantum coherences in the Fenna-Matthew-Olson complex. *arXiv*, 1104.2943.
- [22] Olbrich, C., Strumpfer, J., Schulten, K. & Kleinekathofer U. 2011 Quest for Spatially Correlated Fluctuations in the FMO Light-Harvesting Complex. *J. Phys. Chem. B.*, **115** 758.
- [23] Olbrich, C., & Kleinekathöfer, U. 2011 Time-Dependent Atomistic View on the Electronic Relaxation in Light-Harvesting System II *J. Phys. Chem.* **114**, 12427 - 12437.
- [24] Wending M., Pullerits T., Przyjalowski, M. A. , Vulto, S. I. A., Aartsma, T. J., van Grondelle, R., and van Amerongen, H. 2000 Electron-Vibrational Coupling in the Fenna-Matthews-Olson Complex of Prosthecochloris aestuarii Determined by Temperature-Dependent Absorption and Fluorescence Line-Narrowing Measurements. *J. Phys. Chem.*, **104**, 5825.
- [25] Johnson, S. G. and Small, G. J. 1991 Excited-state structure and energy-transfer dynamics of the bacteriochlorophyll antenna complex from Prosthecochloris aestuarii. *J. Phys. Chem.*, **95**, 471.
- [26] Caycedo-Soler, F., Chin, A.W., Almeida, J., Huelga, S.F., and Plenio, M.B. 2012 The nature of the low energy band of the Fenna-Matthews-Olson complex: vibronic signatures. *E-Print arXiv:1201.0156*
- [27] Brookes, J.C., Hartoutsiou, F., Horsfield, A.P. and Stoneham, A.M. 2007 Could humans recognize odor by phonon assisted tunneling?. *Phys. Rev. Lett.*, **98**, 38101.
- [28] Chin, A.W., Prior, J., Rosenbach, R., Caycedo, F., Huelga, S.F. & Plenio, M.B. 2012 Electronic coherence and recoherence: The role of vibrational structures. *E-print arXiv:1203.0776*
- [29] Hu, X., Ritz, T., Damjanovic, A., Autenrieth, F. and Schulten, K. (2002) Photosynthetic apparatus of purple bacteria. *Q. Rev. Biophys.* **35**, 1 - 62.
- [30] Cogdell, R.J., Gall, A., & Köhler, J. 2006 The architecture and function of the light-harvesting apparatus of purple bacteria: from single molecules to in vivo membranes *Quart. Rev. Biophys.* **39**, 227 - 234.
- [31] Cho, M. 2009 Two-Dimensional Optical Spectroscopy . *C.R.C. Press*.
- [32] Ishizaki, A. & Fleming, G.R. 2009 Theoretical examination of quantum coherence in a photosynthetic system at physiological temperature. *PNAS* **106**, 17255.
- [33] Hayes, D. & Engel, G. S. 2011 Extracting the Excitonic Hamiltonian of the Fenna-Matthews-Olson Complex Using Three-Dimensional Third-Order Electronic Spectroscopy. *Biophys. J.*, **100**, (8), 2043.
- [34] Pachon, L. A. & Brumer, P. 2011 The Physical Basis for Long-lived Electronic Coherence in Photosynthetic Light Harvesting Systems *J. Phys. Chem. Lett.*, **2**, 2728.
- [35] Weiss, U., Quantum Dissipative Systems, World Scientific Singapore 2007.
- [36] We also note that the NIBA approach used in [34] has been applied in a rather different parameter regime than that in which the NIBA is derived, as for Ohmic environments the usual condition for NIBA is that the parameters are in the scaling limit in which the cut-off frequency of the bath ω_c is much larger than all other energy scales in the system. In [34], the tunneling splitting is actually larger than the bath cut-off, which makes the subsequent use of the weak-coupling, biased Markovian theory unreliable, as there is no real separation of system and bath time scales in the problem. Furthermore, the coupling strength used is also not very far into the weak coupling limit required for this theory to be applied.
- [37] Lee, H., Cheng, Y. C. & Fleming, G. R. 2007 Coherence dynamics in photosynthesis: protein protection of excitonic coherence. *Science*, **316**, (5830), 1462.

- [38] Collini, E. & Scholes, G. D. 2009 Coherent intrachain energy migration in a conjugated polymer at room temperature., *Science* **323**, (5912), 369.
- [39] Chin, A. W., S. F. Huelga & Plenio, M. B. 2011 Quantum Metrology in Non-Markovian Environments, *Arxiv:1103.1219*.